A Procedure for the Evaluation of Damping Effects in Composite Laminated Structures

Riccardo Vescovini and Chiara Bisagni*

Dipartimento di Scienze e Tecnologie Aerospaziali, Politecnico di Milano

Via La Masa 34, 20156 Milano, Italy

Abstract

The paper presents an approach based on experimental tests and numerical simulations for taking into account damping effects during the design and the analysis of composite structures. The experiments are conducted using the Dynamic Mechanical Analysis (DMA) and unidirectional coupons are tested to characterize the damping properties of the plies. Starting from these results, first order shear deformation theory is applied to determine the damping properties of the laminate, which are then used in the context of a numerical procedure based on finite element analyses and strain energy method. The results are presented for an aircraft stiffened panel, illustrating the evaluation of the specific damping capacities of the structure, and performing direct transient analyses to investigate the effect of damping on the panel response to pulse loadings.

Keywords: damping, energy dissipation, composite materials.

1 Introduction

Damping is an important aspect related to the behaviour of composite structures. Indeed, the response to dynamic loads is affected by the damping characteristics in terms of vibrations, load distributions and deformed configurations.

While the advantages offered by composite materials are well known with regard to the elastic properties and strength-to-weight ratios, the potentialities related to the damping characteristics have been less investigated. Up-to-date, quite a few methods are available to account for damping effects on composites and, often, the approaches are more of empirical nature. In the context of transient modal dynamic analyses and mode-based steady state dynamic analyses, modal damping is commonly assumed on the basis of the experience or, when available, of experimental tests at sub-component

*Corresponding author. *Email address:* chiara.bisagni@polimi.it (Chiara Bisagni)

or full size level. If this approach is adopted, the inherent contribution to modal damping due to the material cannot be distinguished from that due to joints, frictions and parasitic damping. For this reason, the development of new strategies to quantify the contribution of the material itself to the modal damping is a necessary step to gather insight into the potential benefits offered by the use of composites, and to allow the tailoring of the structures to meet the desired damping properties.

A review of studies on damping in composite materials is found in [1]. In general, two main approaches are found in the literature to characterize the damping of composites: the correspondence principle [2], sometimes referred to as complex-stiffness method or elastic-viscoelastic principle, and the strain energy method [3]. The first of the two approaches consists in converting the linear elastic equations into their viscoelastic counterpart by the substitution of the elastic moduli with the complex ones. The second approach considers the specific damping capacity (SDC) as the ratio between the weighted sum of the energy dissipated by each single element and the total strain energy stored in the structure.

Several works are found in the literature implementing the correspondence principle. Simply supported plates were studied by Alam and Asnani [4] by means of a semi-analytical procedure based on trigonometric expansion of the three displacement components. The formulation was applied to the analysis of plates with cross- and angle-ply lay-ups, and the effects of the material properties, the number of layers and the angles of orientation were investigated. Three different plate theories were considered by Ohta et al. [5] in the context of a procedure based on the corresponding principle and the method of Ritz. The corresponding principle was applied by Meunier and Shenoi [6] to the analysis of sandwich plates, implementing a semi-analytical procedure based on high-order shear deformation theory and Hamilton's principle.

Earlier works on the damping characterization of composite structures based on the strain energy method are the ones of Adams and Bacon [7], and Ni and Adams [8], who represented the energy dissipation by sub-dividing the contributions of the different stress components. The use of the strain energy method was applied by Hwang and Gibson [9] with respect to its application at micro- and macro-mechanical levels. Closed-form expressions were derived by Adams and Maheri [10] for the evaluation of the flexural damping of composite beams using the Adams-Bacon criterion, and the accuracy of the analytical predictions was supported by the comparison with experimental results. Other analytical solutions were developed by Yim and Jang [11] for the analysis of laminated beams. Adams and Maheri [12] derived closed-form solution for the evaluation of dissipative properties of beams, while finite element analyses and the Ritz methods were employed for the study of plates [13, 14].

A comparison between the accuracy of the correspondence principle and the strain energy method is found in the work of Berthelot and Sefrani [15], where the numerical predictions are compared

with the experimental measurements of damping of glass and Kevlar unidirectional composites. The results highlight a good agreement of the strain energy approach with the experiments.

In the context of the various implementations of the strain energy method, a comparative study is presented by Billups and Cavalli [16], where the accuracy of the approaches of Adams and Bacon [7], Ni and Adams [8], Adams and Maheri [12] and Saravanos and Chamis [17, 18] is assessed.

The present work discusses a procedure which can be used to evaluate the modal damping at panel level starting from the experimental characterization of the damping properties at ply level. An overview of the procedure is presented in Figure 1.

The experimental measurements are based on Dynamic Mechanical Analysis (DMA) tests and allow for a quick and convenient characterization of the material properties, while the numerical analysis is faced using the commercial finite element code Abaqus together with Python scripting.

DMA tests are initially performed on unidirectional specimens with different angles of orientations, including on-axis and off-axis configurations. From the experimental results, the damping properties are evaluated at ply level by identifying the specific damping capacities Ψ_{11}, Ψ_{22} and Ψ_{12}. Then, the laminate damping matrices are derived referring to the first order shear deformation theory. At the end of this step, the accuracy of the characterization is checked by comparison of the numerical predictions with the DMA tests performed specimens made by laminates with different plies orientation. The analysis is then performed at panel level. In particular, finite element analyses are conducted to determine the panel SDC as well as the distribution of the dissipated energy. Finally, the modal damping is used in the context of a Rayleigh damping approximation to perform direct transient analyses, and to assess for the effects of damping to a suddenly applied load. In particular, the dynamic buckling behaviour of the panel is investigated referring to the modified Volmir criterion [19]. Indeed, while it is well known that the ratio between the dynamic and the static buckling is usually different from the unity [20–22], the investigation of the effects due to damping have been quite rarely assessed. The Volmir criterion identifies the critical conditions according to the maximum value of the out of plane displacement during the time history, and is consequently affected by the damping properties of the structure.

Compared to other works in the literature, whose focus is the study of beams or plates, the present effort aims to extend the range of applicability of the strain energy method to aircraft sub-component structures. The analysis procedure is developed to account for structures characterized by the presence of regions with different stacking sequences, as well as lay-ups with plies of different materials and/or thicknesses.

Furthermore, the investigation of the dynamic effects on the buckling of the structures has been widely investigated [20–22], but quite rarely the effects of damping have been accounted for.

2 DMA testing

The experimental characterization of the ply damping properties is performed using the DMA. The tests were conducted with the TA Instruments DMA 2980 machine at the laboratory of the Department of Aerospace Science and Technology of Politecnico di Milano.

The DMA is a technique to measure the properties of materials loaded with a periodic stress excitation. During the test, a sinusoidal stress is applied, and the strain is measured. The phase lag between the applied stress and the measured strain is used to estimate the material specific damping capacity, while the amplitudes of the stress and of the strain are used to evaluate the storage and the loss modulus. One of the main advantages of DMA testing is due to the fact that it just requires use of coupons.

The material under investigation is a carbon epoxy. In particular, specimens at 0°, 90°, 30° and 45° are tested, two for each angle of orientation considered.

Various types of fixtures are available for the DMA, such as the three point bending, the single and the dual cantilever configurations. In a previous investigation by Bisagni and Catapano [23], three point bending and dual cantilever configurations were compared, allowing to observe that more reliable results are achieved in terms of specific damping capacity if the cantilever fixture is used. This conclusion is probably due to the non perfect adherence between the specimen and the fixture in the case of three point bending. For this reason, dual cantilever conditions are used in the present investigation. A picture of the DMA equipment is reported in Figure 2 and illustrates the specimen boundary and loading conditions. As seen from the figure, the specimen is fixed at the ends by two screws with a tightening torque of 40 N/mm, while the central probe, which is controlled by a pneumatic system, is responsible for the load introduction.

The overall dimensions of the specimens are 60 $mm \times 10$ mm, while the effective length, measured as the clamp-to-clamp distance, is 37.5 mm.

The coupons are realized by the stacking of six plies of unidirectional material with same angle of orientations, for a nominal thickness equal to 0.75 mm, as the result of the stacking of six plies of thickness 0.125 mm. In general, the testing of single-ply specimens would be preferable in order to minimize the contribution of the transverse shear compliance to the dissipated energy. However, practical limitations exist on the maximum and minimum stiffness of the specimen to be tested. For this reason, a number of six plies is chosen to guarantee that the bending stiffness of the specimens falls in the machine operating range. In particular, the range of equivalent bending stiffnesses that can be tested is between 10^{-1} and 10^{4} N/mm. The actual stiffness of the specimens is estimated assuming a clamped-clamped beam model, where the load is introduced with a transversely applied force in the middle. The tests are performed with a sinusoidal amplitude-controlled mode, where the

maximum amplitude is fixed to 15 μm, a value that guarantees the specimen to operate in the small vibrations range.

The tests are performed with the frequency range between 0.5 and 50 Hz, with 9 points per decade. At the beginning of the test, an isothermal soak of 5 minutes is kept to guarantee a homogeneous temperature distribution of 35 $^{\circ}C$ within the sample. The temperature of 35 $^{\circ}C$ is chosen to obtain results close to the room conditions of typical tests at panel level. After completing the temperature step, the machine starts the loading cycles.

The equivalent bending stiffness of the specimen is obtained as:

$$K = \frac{24EJ}{a^3\left[1 + \frac{E_{\text{eq}}}{\chi G_{\text{eq}}}\left(\frac{t}{a}\right)^2\right]} \tag{1}$$

where E_{eq} and G_{eq} are the laminate equivalent Young's and shear moduli, EJ is the bending stiffness, χ is the shear factor, t is the laminate thickness and a is half of the beam length.

The equivalent moduli are obtained as [24]:

$$E_{\text{eq}} = \frac{A_{11}A_{22} - A_{12}^2}{tA_{22}} \qquad G_{\text{eq}} = \frac{A_{66}}{t} \tag{2}$$

where the terms A_{ik} are the elastic in-plane stiffness of the laminate, according to Voigt notation. Table 1 summarizes the stiffness K for different angles of orientation of the specimen, showing that all the values fall within the machine operating range. It is worth noting that the shear contribution is relevant for the specimen at 0°. If shear flexibility is neglected, the equivalent bending stiffness is overestimated of about 7%. On the other hand, the shear contribution is negligible for the other three specimens.

The results of the tests are reported in Figure 3 for the eight unidirectional specimens, where the measured specific damping capacity Ψ is reported versus the frequency. The damping capacity is defined as:

$$\Psi = \frac{\Delta U}{U_{\text{tot}}} \tag{3}$$

where ΔU is the strain energy dissipated during a cycle, and U_{tot} is the maximum strain energy stored during the cycle.

The specific damping capacity Ψ is related to the loss factor η and the modal damping ξ through the expression:

$$\Psi = 2\pi\eta = 4\pi\xi \tag{4}$$

As revealed by the experimental results of the four configurations, the lowest values of SDC are associated to the specimen at 0°. Indeed, the response of this specimen is governed by the bending of the fibers. On the other hand, higher dissipation is observed for the off-axis specimens, where the contribution of the viscoelastic matrix is predominant. The dissipated energy depends on the

frequency of excitation and, for certain levels, the highest dissipation is observed in the 45° specimen, while for others in the 90° specimen.

3 Ply damping properties

The ply damping properties are defined by the specific damping capacities Ψ_{11}, Ψ_{22} and Ψ_{12}. The first two contributions are related to the damping in the direction of the fibers and transverse to them, while the third term expresses the specific damping capacity due to shear deformations.

The DMA testing provides the specific damping capacity Ψ^θ for each specimen oriented at θ degrees. The quantities measured from two specimens at 0° and 90° are, with a good degree of approximation, equal to the specific damping capacities Ψ_{11} and Ψ_{22}. Indeed, the deformations during the loading cycles are governed by the single contributions of the fibers and the matrix, respectively. Contrarily, the damping capacity measured from the specimens at 30° and 45° is not equal to the shear damping Ψ_{12}, as the corresponding deformed configurations involve a combination of fiber, matrix and shearing modes. These measured damping capacities are used to determine the value of Ψ_{12}. One possibility is given by the analytical model proposed by Melo and Radford [25]:

$$\Psi_{12} = \frac{G_{12}}{\sin(\theta)^2 \cos(\theta)^2} \left[\Psi^\theta \frac{1}{E_{\theta\theta}} - \frac{\Psi_{11}}{E_{11}} \cos(\theta)^4 - \frac{\Psi_{22}}{E_{22}} \sin(\theta)^4 + \sin(\theta)^2 \cos(\theta)^2 \left(\Psi_{11} + \Psi_{22}\right) \frac{\nu_{12}}{E_{11}} \right] \quad (5)$$

where E_{11}, E_{22} and G_{12} are the material Young's and shear moduli, E_θ and Ψ^θ are the storage modulus and the specific damping capacity of the specimen at θ degrees, respectively.

While this approach offers the advantage of providing a solution in closed-form, it suffers from the limitation of relying on the assumption of a uniform state of uniaxial stress within the specimen. In general, this is a good approximation for the coupons at 0° and 90°, but it is not true in the case of the configurations at 30° and 45°. Indeed, the material anisotropy, consisting both in membrane/shear and bending/twisting couplings, determines a non-uniform stress distribution within the specimen. These effects are negligible for length-to-width ratios of the order of 10 to 20, as remarked in Ref. [26], but the specimens under investigation are characterized by ratios well below 10. To overcome these limitations, a strategy is here discussed, based on the finite element simulation of the DMA test. In particular, the stress distribution is evaluated numerically, thus avoiding the introduction of the assumption of uniform uniaxial stress.

The analyses are performed with the commercial code Abaqus, and four-noded S4R shell elements are used for the discretization. An example of the finite element model of the specimen is reported in Figure 4. The external edges are clamped by constraining all the degrees of freedom, while the row of nodes in the middle is subjected to an imposed displacement to simulate the movement of the

central probe. A mesh size of 1 $mm \times 1\ mm$ is chosen on the basis of a preliminary convergence analysis.

The evaluation of the energy dissipation is performed referring to the damping criterion proposed by Adams-Bacon. It states that the dissipation of a thin laminate can be determined as the sum of the separable contribution due to the three in-plane stress/strain components, i.e in the fiber direction, in the direction transverse to the fibers and in-plane shear, and the transverse shear components. The energy dissipation is quantified by means of the specific damping capacity, as defined in Eq. (3). The same expression can be re-written in terms of energy densities as:

$$\Psi = \frac{\int_V \Delta u \, dV}{\int_V u_{\text{tot}} \, dV} \tag{6}$$

where V is the volume of the structure, Δu and u_{tot} are the dissipated and the strain energy densities per unit volume, respectively. In particular, the application of the Adams-Bacon criterion allows to re-write the dissipated energy Δu of Eq. (6) as:

$$\begin{aligned} \Delta u &= \Psi_{11} u_{11} + \Psi_{22} u_{22} + \Psi_{12} u_{12} + \Psi_{13} u_{13} + \Psi_{23} u_{23} \\ &= \Delta u_{11} + \Delta u_{22} + \Delta u_{12} + \Delta u_{13} + \Delta u_{23} \end{aligned} \tag{7}$$

while the total strain energy reads:

$$u_{tot} = u_{11} + u_{22} + u_{12} + u_{13} + u_{23} \tag{8}$$

where:

$$u_{11} = \frac{1}{2}\sigma_{11}\varepsilon_{11} \qquad u_{22} = \frac{1}{2}\sigma_{22}\varepsilon_{22} \qquad u_{12} = \frac{1}{2}\sigma_{12}\gamma_{12} \tag{9}$$

$$u_{13} = \frac{1}{2}\sigma_{13}\gamma_{13} \qquad u_{23} = \frac{1}{2}\sigma_{23}\gamma_{23} \tag{10}$$

and the terms σ_{11}, σ_{22}, σ_{12}, σ_{13}, σ_{23} denote the components of the stress tensor expressed in the lamina coordinate system, and similarly for the corresponding strain components. The shear strains γ_{ik} are defined as:

$$\gamma_{ik} = 2\epsilon_{ik} \tag{11}$$

The transverse shear strains γ_{13} and γ_{23} are not available in the Abaqus output file, but they can be easily obtained from the rotation of the strains in laminate coordinate γ_{xz} and γ_{yz} as:

$$\gamma_{13} = \cos\theta\gamma_{xz} + \sin\theta\gamma_{yz} \qquad \gamma_{23} = -\sin\theta\gamma_{xz} + \cos\theta\gamma_{yz} \tag{12}$$

In the context of the finite element discretization, the SDC of Eq. (6) is obtained as the sum of the energy stored in each single finite element, so:

$$\Psi = \frac{\sum_{e=1}^{\text{N}_{\text{el}}} \int_{\text{v}_\text{e}} \left(\Psi_{11} u_{11}^e + \Psi_{22} u_{22}^e + \Psi_{12} u_{12}^e + \Psi_{13} u_{13}^e + \Psi_{23} u_{23}^e\right) \, d\text{v}_\text{e}}{\sum_{e=1}^{\text{N}_{\text{el}}} \int_{\text{v}_\text{e}} \left(u_{11}^e + u_{22}^e + u_{12}^e + u_{13}^e + u_{23}^e\right) \, d\text{v}_\text{e}} = \frac{\sum_{e=1}^{\text{N}_{\text{el}}} \Delta U^e}{\sum_{e=1}^{\text{N}_{\text{el}}} U^e} \tag{13}$$

where $\mathrm{N_{el}}$ is the number of elements and $\mathrm{v_e}$ is the volume of the generic finite element e.

The strain energy contribution U_{ij}^e of the generic element e is obtained after integration of the strain energy density over the element volume as:

$$U_{ij}^e = \int_{\mathrm{v_e}} u_{ij}^e \, d\mathrm{v_e} = \int_{\mathrm{A_{el}}} \sum_{k=1}^{\mathrm{N_{plies}}} \int_{z_k}^{z_{k+1}} u_{ij}^e \, dz \, dA_{\mathrm{el}} \tag{14}$$

where $\mathrm{N_{plies}}$ is the number of plies composing the laminate of the element e, and $\mathrm{A_{el}}$ is the corresponding area. it is remarked that the material coupons used in the present investigation are obtained form the stacking of six plies, so $\mathrm{N_{plies}} = 6$.

The mesh is realized with S4R elements that use reduced in-plane integration. Therefore both the strains and the stresses are constant within the element domain. The surface integration is then performed by multiplying the terms of Eqs. (9) and (10) by the element area, while the integration along the thickness direction is performed using the Simpsons's rule, i.e.:

$$U_{ij}^e = \frac{A_{\mathrm{el}}}{6} \sum_{k=1}^{N_{\mathrm{plies}}} t_{\mathrm{ply}}^{(k)} \left[u_{ij}^e(z_1^{(k)}) + 4u_{ij}^e(z_2^{(k)}) + u_{ij}^e(z_3^{(k)}) \right] \tag{15}$$

where $z_1^{(k)}$, $z_2^{(k)}$ and $z_3^{(k)}$ are the thicknesswise coordinates of the three integration points of the generic layer k. Similarly, the dissipated energy becomes:

$$\Delta U_{ij}^e = \frac{A_{\mathrm{el}}}{6} \sum_{k=1}^{N_{\mathrm{plies}}} t_{\mathrm{ply}}^{(k)} \Psi_{ij}^{(k)} \left[u_{ij}^e(z_1^{(k)}) + 4u_{ij}^e(z_2^{(k)}) + u_{ij}^e(z_3^{(k)}) \right] \tag{16}$$

The expressions of Eqs. (15) and (16) highlight the need for performing the integration along the thickness by summing the contribution of each single ply.

Recalling that Ψ^θ is the experimental specific damping capacity of the specimen at θ degrees and using Eqs. (6), (7) and (8), it is possible to write:

$$\Psi^\theta = \frac{U_{11}^\theta \Psi_{11} + U_{22}^\theta \Psi_{22} + U_{12}^\theta \Psi_{12} + U_{23}^\theta \Psi_{23} + U_{13}^\theta \Psi_{13}}{U_{\mathrm{tot}}^\theta} \tag{17}$$

where the terms Ψ_{ik} are the five unknown specific damping capacities of the ply, while U_{ik}^θ and U_{tot}^θ are the strain energies, computed with the finite elements, corresponding to the maximum cycle deformation during the DMA test. In the expression U_{ik}^θ, the subscripts denote the strain energy contribution, while the superscripts refer to the orientation of the specimen.

Under the assumption of transversely isotropic material, the number of unknown parameters can be reduced from five to three, and Eq. (17) is given by:

$$\Psi^\theta = \frac{\left(U_{11}^\theta + U_{13}^\theta\right) \Psi_{11} + \left(U_{22}^\theta + U_{23}^\theta\right) \Psi_{22} + U_{12}^\theta \Psi_{12}}{U_{\mathrm{tot}}^\theta} \tag{18}$$

The expression of Eq. (18) can be written for each coupon configuration tested with the DMA, so leading to a system of linear equations in the form:

$$\mathbf{A}\boldsymbol{\Psi} = \boldsymbol{\Psi}^{\mathrm{exp}} \tag{19}$$

where the vector of unknowns is defined as:

$$\mathbf{\Psi} = \left\{ \Psi_{11} \quad \Psi_{22} \quad \Psi_{12} \right\}^T \tag{20}$$

The right-hand side of Eq. (19) is a vector collecting the specific damping capacities Ψ^θ as measured from the testing of the specimens at 0°, 30°, 45° and 90°:

$$\mathbf{\Psi}^{\exp} = \left\{ \Psi^0 \quad \Psi^{30} \quad \Psi^{45} \quad \Psi^{90} \right\}^T \tag{21}$$

The matrix of coefficients $\mathbf{A}$ of Eq. (19) is:

$$\mathbf{A} = \begin{bmatrix} U_{11}^0 + U_{13}^0 & U_{22}^0 + U_{23}^0 & U_{12}^0 \\ U_{11}^{30} + U_{13}^{30} & U_{22}^{30} + U_{23}^{30} & U_{12}^{30} \\ U_{11}^{45} + U_{13}^{45} & U_{22}^{45} + U_{23}^{45} & U_{12}^{45} \\ U_{11}^{90} + U_{13}^{90} & U_{22}^{90} + U_{23}^{90} & U_{12}^{90} \end{bmatrix} \tag{22}$$

where the terms of Eq. (22) are obtained numerically from the finite element simulation of the DMA test.

As far as the number of experimental tests is equal to four, while the number of unknowns is equal to three, the linear system of Eq. (19) is overdetermined. The solution is then performed using the minimum least squares obtaining the three specific damping capacities of Eq. (20).

4 Laminate damping matrices

The availability of the damping properties at ply level allows, in principle, to compute the specific damping capacity of any arbitrarily complex structure. In particular, the SDC of the structure can be evaluated, starting from the values of Ψ_{11}, Ψ_{22} and Ψ_{12}, referring to Eq. (13). This expression requires the computation of a volume integral for each element of the finite element model and determines a significant CPU effort due to the need for computing the strain energy density ply by ply, as it can be observed from Eqs. (15) and (16). A more effective approach consists in modeling the damping properties at laminate level, starting from the properties at ply level.

The relevant equations to determine the laminate damping matrices are here derived starting from the expression of the dissipated energy density of the element e. In particular, using Eqs. (9), (10) and (13):

$$\begin{aligned} \Delta U^e = \frac{1}{2} \int_{\mathrm{A_{el}}} \sum_{k=1}^{\mathrm{N_{plies}}} \int_{z_k}^{z_{k+1}} \Big(& \sigma_1^{(k)} \epsilon_1^{(k)} + \sigma_2^{(k)} \epsilon_2^{(k)} + \tau_{12}^{(k)} \gamma_{12}^{(k)} + \tau_{13}^{(k)} \gamma_{13}^{(k)} + \\ & + \tau_{23}^{(k)} \gamma_{23}^{(k)} \Big) \, dz \, d\mathrm{A_{el}} \end{aligned} \tag{23}$$

The expression of Eq. (23) is re-written in matrix notation as:

$$\begin{aligned}\Delta U^e =& \frac{1}{2}\int_{\mathrm{A_{el}}}\sum_{k=1}^{N_{\mathrm{plies}}}\int_{z_k}^{z_{k+1}} {\boldsymbol{\epsilon}_1^{(k)}}^T \mathrm{diag}[\Psi^{(k)}]\boldsymbol{\sigma}_1^{(k)}\, dz\, d\mathrm{A_{el}} + \\ &+\frac{1}{2}\int_{\mathrm{A_{el}}}\sum_{k=1}^{N_{\mathrm{plies}}}\int_{z_k}^{z_{k+1}} {\boldsymbol{\gamma}_1^{(k)}}^T \mathrm{diag}[\Psi_s^{(k)}]\boldsymbol{\tau}_1^{(k)}\, dz\, d\mathrm{A_{el}}\end{aligned} \tag{24}$$

where the in-plane and transverse strains are collected in the vectors $\boldsymbol{\epsilon}_1^{(k)}$ and $\boldsymbol{\gamma}_1^{(k)}$, which are defined as:

$$\boldsymbol{\epsilon}_1^{(k)} = \{\epsilon_1 \quad \epsilon_2 \quad 2\epsilon_{12}\}^T \qquad\qquad \boldsymbol{\gamma}_1^{(k)} = \{\gamma_{13} \quad \gamma_{23}\}^T \tag{25}$$

Accordingly, the in-plane and transverse stresses $\boldsymbol{\sigma}_1^{(k)}$ and $\boldsymbol{\tau}_1^{(k)}$ of the k-th ply are:

$$\boldsymbol{\sigma}_1^{(k)} = \{\sigma_1 \quad \sigma_2 \quad \tau_{12}\}^T \qquad\qquad \boldsymbol{\tau}_1 = \{\tau_{13} \quad \tau_{23}\}^T \tag{26}$$

The first term of Eq. (24) is related to the in-plane behaviour of the laminate, while the second term accounts for the response in the transverse direction.

The material specific damping capacities, obtained from the solution of Eq. (19), are organized in diagonal matrices as:

$$\mathrm{diag}[\Psi^{(k)}] = \begin{bmatrix} \Psi_{11}^{(k)} & 0 & 0 \\ 0 & \Psi_{22}^{(k)} & 0 \\ 0 & 0 & \Psi_{12}^{(k)} \end{bmatrix} \qquad \mathrm{diag}[\Psi_s^{(k)}] = \begin{bmatrix} \Psi_{11}^{(k)} & 0 \\ 0 & \Psi_{22}^{(k)} \end{bmatrix} \tag{27}$$

where the terms of the matrix $\Psi_s^{(k)}$ rely on the assumption of transversely isotropic behaviour of the material.

The superscript k in the matrix terms denotes that, in principle, the specific damping capacities can be different from ply to ply.

The constitutive equation for the k-th ply, expressed in the lamina reference system, is:

$$\boldsymbol{\sigma}_1^{(k)} = \mathbf{C}^{(k)}\boldsymbol{\epsilon}_1^{(k)} \qquad\qquad \boldsymbol{\tau}_1^{(k)} = \mathbf{C}_s^{(k)}\boldsymbol{\gamma}_1^{(k)} \tag{28}$$

where the matrices $\mathbf{C}^{(k)}$ and $\mathbf{C}_s^{(k)}$ have the following expressions:

$$\mathbf{C}^{(k)} = \begin{bmatrix} \frac{E_1}{1-\nu_{12}\nu_{21}} & \frac{\nu_{12}E_2}{1-\nu_{12}\nu_{21}} & 0 \\ \frac{\nu_{12}E_2}{1-\nu_{12}\nu_{21}} & \frac{E_2}{1-\nu_{12}\nu_{21}} & 0 \\ 0 & 0 & G_{12} \end{bmatrix} \qquad \mathbf{C}_s^{(k)} = \begin{bmatrix} G_{13} & 0 \\ 0 & G_{23} \end{bmatrix} \tag{29}$$

The relation between the strain components expressed in lamina and laminate coordinate system is:

$$\boldsymbol{\epsilon}_1^{(k)} = \mathbf{T}\boldsymbol{\epsilon}_x \qquad\qquad \boldsymbol{\gamma}_1^{(k)} = \mathbf{T}_s\boldsymbol{\gamma}_x \tag{30}$$

where the matrices $\mathbf{T}$ and $\mathbf{T}_s$ are:

$$\mathbf{T} = \begin{bmatrix} c^2 & s^2 & sc \\ s^2 & c^2 & -sc \\ -2cs & 2cs & c^2 - s^2 \end{bmatrix} \qquad \mathbf{T}_s = \begin{bmatrix} c & -s \\ s & c \end{bmatrix} \tag{31}$$

with c and s denoting the sine and the cosine of the ply angle.

After substitution of Eq. (30) into Eq. (24), the expression of the dissipated energy becomes:

$$\begin{aligned} \Delta U^e = \frac{1}{2} \int_{\mathrm{A_{el}}} \sum_{k=1}^{N_{\mathrm{plies}}} \int_{z_k}^{z_{k+1}} \boldsymbol{\epsilon}_x^T \mathbf{T}^T \mathrm{diag}[\Psi^{(k)}] \mathbf{C}^{(k)} \mathbf{T} \boldsymbol{\epsilon}_x dz \, d\mathrm{A_{el}} + \\ + \frac{1}{2} \int_{\mathrm{A_{el}}} \sum_{k=1}^{N_{\mathrm{plies}}} \int_{z_k}^{z_{k+1}} \boldsymbol{\gamma}_x^T \mathbf{T}_s^T \mathrm{diag}[\Psi_s^{(k)}] \mathbf{C}_s^{(k)} \mathbf{T}_s \boldsymbol{\gamma}_x dz \, d\mathrm{A_{el}} \end{aligned} \tag{32}$$

The expression of Eq. (32) highlights the possibility of building the laminate damping matrices in analogy with the elastic ones. Indeed, an equivalent constitutive law can be defined as:

$$\tilde{\mathbf{C}}^{(k)} = \mathrm{diag}[\Psi^{(k)}] \mathbf{C}^{(k)} \qquad \tilde{\mathbf{C}}_s^{(k)} = \mathrm{diag}[\Psi_s^{(k)}] \mathbf{C}_s^{(k)} \tag{33}$$

The procedure here presented is based on the first order shear deformation theory. Under this assumption, the relation between the strains $\boldsymbol{\epsilon}_x$ and $\boldsymbol{\gamma}_x$ at the generic coordinate z and the strains $\boldsymbol{\epsilon}_0$ and $\boldsymbol{\gamma}_0$ of the mid-surface is [26]:

$$\boldsymbol{\epsilon}_x = \boldsymbol{\epsilon}_0 + z\mathbf{k} \qquad \boldsymbol{\gamma}_x = \boldsymbol{\gamma}_0 \tag{34}$$

where $\mathbf{k}$ is the vector of the laminate curvatures.

The expression of Eq. (34) can be substituted into Eq. (32) and, after performing the integration along the direction z, it is obtained:

$$\Delta U^e = \frac{1}{2} \int_{\mathrm{A_{el}}} \begin{Bmatrix} \boldsymbol{\epsilon}_0 \\ \mathbf{k} \end{Bmatrix}^T \begin{bmatrix} \tilde{\mathbf{A}} & \tilde{\mathbf{B}} \\ \tilde{\mathbf{B}} & \tilde{\mathbf{D}} \end{bmatrix} \begin{Bmatrix} \boldsymbol{\epsilon}_0 \\ \mathbf{k} \end{Bmatrix} d\mathrm{A_{el}} + \frac{1}{2} \chi \int_{\mathrm{A_{el}}} \boldsymbol{\gamma}_0^T \tilde{\mathbf{A}}_s \boldsymbol{\gamma}_0 \, d\mathrm{A_{el}} \tag{35}$$

where the matrices $\tilde{\mathbf{A}}$, $\tilde{\mathbf{B}}$, $\tilde{\mathbf{D}}$ and $\tilde{\mathbf{A}}_s$ characterize the damping response of the laminate, while χ is the shear factor. The expression of the four matrices is equal to the one of the elastic stiffnesses obtained in the context of the first order shear theory. The only difference consists in the use of the equivalent constitutive laws of Eq. (33) instead of the ply constitutive law of Eq. (28). The relevant equations are:

$$\begin{aligned} \tilde{\mathbf{A}} &= \sum_{k=1}^{N_{\mathrm{plies}}} \mathbf{T} \tilde{\mathbf{C}}^{(k)} \mathbf{T}^T \left(z_{k+1} - z_k \right) & \tilde{\mathbf{B}} &= \frac{1}{2} \sum_{k=1}^{N_{\mathrm{plies}}} \mathbf{T} \tilde{\mathbf{C}}^{(k)} \mathbf{T}^T \left(z_{k+1}^2 - z_k^2 \right) \\ \tilde{\mathbf{D}} &= \frac{1}{3} \sum_{k=1}^{N_{\mathrm{plies}}} \mathbf{T} \tilde{\mathbf{C}}^{(k)} \mathbf{T}^T \left(z_{k+1}^3 - z_k^3 \right) & \tilde{\mathbf{A}}_s &= \sum_{k=1}^{N_{\mathrm{plies}}} \mathbf{T} \tilde{\mathbf{C}}_s^{(k)} \mathbf{T}^T \left(z_{k+1} - z_k \right) \end{aligned} \tag{36}$$

It is observed that the expressions of Eq. (36) can be computed just once, at the beginning of the procedure. Then, the evaluation of the dissipated energy, as reported in Eq. (35), does not require the integration along the thickness direction, as in the case of Eq. (16), and can be performed with a reduced computational effort. Another advantage consists in the reduced amount of data to be written in the output file, as only the midsurface strains and curvatures are required.

The elastic strain energy of the generic element e, which is derived from the first order laminate theory, assumes the well-known expression:

$$U^e = \frac{1}{2}\int_{\mathrm{A_{el}}} \begin{Bmatrix} \boldsymbol{\epsilon}_0 \\ \mathbf{k} \end{Bmatrix}^T \begin{bmatrix} \mathbf{A} & \mathbf{B} \\ \mathbf{B} & \mathbf{D} \end{bmatrix} \begin{Bmatrix} \boldsymbol{\epsilon}_0 \\ \mathbf{k} \end{Bmatrix} d\mathrm{A_{el}} + \frac{1}{2}\chi \int_{\mathrm{A_{el}}} \boldsymbol{\gamma}_x^T \mathbf{A}_s \boldsymbol{\gamma}_x \, d\mathrm{A_{el}} \tag{37}$$

The specific damping capacity of the overall structure is finally derived substituting Eqs. (35) and (37) into Eq. (13).

it is finally remarked that the procedure here outlined do not account for the effects of interlaminar resin-rich regions on the overall damping. This contribution is assumed to be negligible for the thin laminates here under investigation. To validate the procedure, two specimens obtained from the stacking of eight plies at $[45/90/\text{-}45/0]_s$ were manufactured and tested with the DMA. The specific damping capacities were then compared with those obtained numerically referring to Eqs. (35) and (37). .

The results of Figure 5 report the comparison between the experimental specific damping capacity, and the numerical one. It is observed that the dissipated energy is well predicted especially at the lowest frequencies, until the value of 15 Hz. An overestimation of the damping capacity is then observed in the range of frequencies between 20 and 35 Hz, probably as the result of resonance phenomena on the unidirectional specimens used to characterize the damping. Good agreement is then observed beyond 40 Hz. In general, the comparison can be considered satisfactory, especially considering the several uncertainties related to the environmental conditions, small specimen misalignments and machine calibration issues that typically affect the results of the test.

5 Analysis of a panel

The analysis procedure at panel level is illustrated in Figure 6. Abaqus eigenvalue analysis are firstly performed on the structure, and the results, in terms of modal strains, are written in a binary file. The computation of the SDC is performed starting from the results of the eigenvalue analysis. In particular, the eigenstrains are used to compute the strain energy according to Eq. (35) and, together with the laminate damping matrices, to determine the dissipated energy according to Eq. (37). It is observed that the laminate damping matrices are computed starting from the SDC at ply level

obtained from DMA tests. The specific damping capacity of the panel is then obtained according to Eq. (3). A Python script is implemented to read the results and compute the panel specific damping capacity. The script allows also to write the results into the Abaqus binary output file. Indeed, the results allow to visualize how the energy is distributed within the different structural areas. This aspect is particularly useful to obtain insight into the damping behavior of the structure, and can provide useful information during the design phase. For instance, it identifies the most suitable regions to maximize the effect of interleaved viscoelastic layers or damping treatments.

Transient dynamic analysis can be performed after introducing the Rayleigh damping approximation, and using the panel SDC to build the damping matrix.

5.1 Panel description

The procedure is applied to study a typical aircraft composite panel investigated within the DAEDALOS project. The panel has a radius of curvature of 980 mm, an arc-length of 310 mm and is 720 mm long. It is stiffened by three blade stringers, whose height is 20 mm. The connection between the skin and the stringers is obtained by means of two flanges of 20 mm each. A sketch of the panel is reported in Figure 7.

The material is carbon/epoxy T800/M21, whose elastic properties are summarized in Table 2. The nominal ply thickness is equal to 0.125 mm.

The skin is layered with quasi-isotropic stacking sequence $[0/\text{-}45/45/90]_s$, corresponding to a total thickness of 1 mm. The lay-up of the stiffener web is $[\text{-}45/45/0/0]_{3s}$, for a total thickness of 3 mm. The region of overlap between the skin and the stiffener foot is obtained as the superposition of the skin and half of the stiffener lay-ups.

The ply damping properties are the ones measured with the DMA testing. As the machine could not reach frequency values beyond 50 Hz, the damping properties at higher frequency values are conservatively assumed to be equal to those measured at 50 Hz.

The values are summarized in Table 3, and are of the same order of magnitude of values found in the literature [25, 27] for similar composite materials.

The finite element model of the panel is realized using S4R shell elements of dimensions 3 mm $\times$ 3 mm, on the basis of a preliminary convergence study. The lateral edges of the panel are free. The three displacement components are constrained at the one of the two transverse edges, while all but the axial displacement components are constrained at the second edge.

5.2 Specific damping capacity

The results of the eigenanalysis and the strain energy method are reported in Figure 8 for the first vibration mode, where the contour of the out of plane displacement and the dissipated energy density are presented. The specific damping capacity of the panel is equal to 2.1%. From Figure 8(a), it is observed that the first eigenvector, associated to a frequency of 169 Hz, is characterized by out of plane displacements that involve mainly the deflection of the skin. Contrarily, it is clear from Figure 8(b) that the most significant contribution to the energy dissipation is due to local stiffener deflections. In particular, the peaks of the dissipated energy density are visible on few localized positions of the stiffener web, while the density amplitudes on the other portions of the skin are much smaller, resulting in an almost homogenous contour.

A representation of the dissipative properties of the structure is reported in Figure 9. The graphic reveals the different contributions due to the skin, the foot and the stiffener to overall the specific damping capacity. The skin and the stiffener foot dissipate mainly in the fiber bending mode. In both cases, the contribution due to the deformations in the direction transverse to the fibers is almost null and only a small amount of dissipation is achieved thanks to shear deformations. The portion of structure providing the highest contribution to the overall dissipation is the stiffener, as visible also from the contour of Figure 8(b). The contributions of the transverse shear deformations are not reported in Figure 9, as they are small in comparison to others. Indeed, only 0.5% of the total strain energy is due to the energy term U_{13}, and 0.8% to the term U_{23}.

The results of the strain energy method are illustrated in Figure 10 for the first six eigenmodes, and the contribution of each portion of the structure to the overall dissipation is highlighted. It can be seen that the specific damping capacities of the first six modes is approximately constant, with values around 2%. However, the dissipation is achieved with combinations of energy contributions that are, in general, different for each mode. In particular, the most significant contribution of the first mode is the one of the stiffeners, while the foot and the skin are responsible for a minor amount of dissipation. The contribution of the skin tends to increase with the mode number and, for the fifth and sixth mode, the dissipation due to the skin is higher than the one due to the stiffener.

5.3 Transient analysis

The effect of damping on the response of the panel subjected to suddenly applied loads is here investigated. The approach is based on the direct time integration of the equations, where geometrical nonlinearities are accounted for. The governing equations of motion are expressed in physical

coordinates, and assume the well-known expression [28]:

$$\mathbf{M}\ddot{\mathbf{x}}^{t+\Delta t} + \mathbf{C}\Delta\dot{\mathbf{x}} + (\mathbf{K_L} + \mathbf{K_{NL}})\,\Delta\mathbf{x} = \mathbf{R}^{t+\Delta t} - \mathbf{F}^{t} \tag{38}$$

where $\mathbf{M}$, $\mathbf{C}$ and $\mathbf{K}$ are the mass, the damping and the stiffness matrices, respectively. The vector $\ddot{\mathbf{x}}^{t+\Delta t}$ collects the nodal accelerations at time $t + \Delta t$, the vectors $\Delta\dot{\mathbf{x}}$ and $\Delta\mathbf{x}$ are the vectors of increments of nodal velocity and displacement, respectively. The term $\mathbf{R}^{t+\Delta t}$ is the vector of external loads, while $\mathbf{F}(t)$ is the vector of internal loads. The damping matrix $\mathbf{C}$ is determined referring to the Rayleigh model, using as inputs the specific damping capacities obtained at panel level. The Rayleigh damping model has been widely used to determine the viscous damping matrix $\mathbf{C}$ [29, 30], and is available in most of the commercial finite element codes. The main idea of the Rayleigh approximation consists in assuming the viscous damping matrix as the weighted sum of the mass and stiffness matrices:

$$\mathbf{C} = \alpha\mathbf{M} + \beta\,(\mathbf{K_L} + \mathbf{K_{NL}}) \tag{39}$$

where the coefficients α and β are the proportional coefficients. One strategy to determine the values of α and β is suggested by Riks et al. [29]:

$$\alpha = \omega_1 \frac{\Psi_1}{4\pi} \qquad \beta = \frac{\Psi_1}{4\pi\omega_1} \tag{40}$$

where Ψ_1 is the SDC associated to the first eigenmode, and ω_1 is the lowest angular eigenfrequency. Compared to the approach of Riks et al. [29], where the SDC Ψ_1 is arbitrarily chosen in the range from 0.6 and 2.5, the present approach considers the value of Ψ_1 as obtained from the evaluation of the panel SDC.

Denoting with $\mathbf{q}_i$ the i-th eigenmode, the modal damping is:

$$\mathbf{q}_i^T \mathbf{C} \mathbf{q}_i = \omega_i \frac{\Psi_i}{2\pi} \tag{41}$$

where ω_i is the angular frequency of the i-th undamped mode.

Substituting Eq. (39) into the left-hand side of Eq. (41), and assuming that the eigenvectors are normalized such that $\mathbf{q}_i^T\mathbf{M}\mathbf{q}_i = 1$ and $\mathbf{q}_i^T\mathbf{K}\mathbf{q}_i = \omega_i^2$, it is obtained:

$$\alpha + \beta\omega_i = \omega_i \frac{\Psi_i}{2\pi} \tag{42}$$

The comparison between Eqs. (40) and (42) highlights that the Rayleigh approximation provides a correct representation of the modal damping associated to the generic i-th vibrating mode. On the other hand, the contribution proportional to the mass determines a damping term that increases linearly with the frequency, while the term proportional to the stiffness provides a value that is inversely proportional to the frequency. Therefore, exact correspondence with the damping values obtained with the strain energy method is achieved only for the i-th mode of vibration, which is chosen by

the user at beginning of the procedure. In the analyses reported in the next, the first eigenmode has been considered.

The dynamic analyses are performed using the Abaqus implicit solution procedure, where geometric nonlinearties are accounted for. Goal of the procedure is the investigation of the response in presence of impulsive axial loads, which can trigger dynamic buckling phenomena. It is recalled that dynamic buckling is not related to a bifurcation phenomenon, as it happens in the static case. It follows that the definition of the critical conditions is not unique. Among the different criteria proposed in the literature, a dynamic buckling condition based on the maximum out of plane displacement is here adopted. Indeed, during the design phase, the maximum out of plane displacement corresponding to the static buckling condition is often taken as reference value, and is used to compare the entity of the deflections observed in case of dynamic loading [31]. In particular, an information of practical interest is the amount of axial displacement, for different pulse durations, leading to a maximum out of plane deflections equal to the one obtained in static buckling conditions. This criterion is sometimes referred to as modified Volmir criterion [19].

The panel is loaded by imposing an axial shortening δ at one of the two ends with the time history of Figure 11. At the beginning, the value of δ is progressively increased from zero to $\delta_{\max}$ with a transient phase of 0.1 T, where T denotes the overall time period. Once the regime value $\delta_{\max}$ is reached, the load is kept constant for an amount of time of 0.8 T. Then, it is removed in the timeframe from 0.9 T to T.

The pulse time durations T here considered are in the range between 1 and 20 ms. For each of them, several analyses are repeated by progressively increasing the regime value of $\delta_{\max}$, until the static buckling out of plane displacement is reached.

The results of the dynamic analysis are reported in Figure 12 for various time durations, considering both the damped and the undamped cases. Each point of the two curves is obtained from a serie of analyses performed at fixed load duration, but increasing applied displacement. The horizontal line corresponds to the static buckling condition. The dynamic load factor reported in Figure 12 is defined as the ratio between the dynamic shortening $\overline{\delta}$ and the axial shortening δ_{cr} corresponding to static buckling conditions, i.e. 0.64 mm. The nondimensional representation of the results, which reports the dynamic load factor versus the time pulse durations, provides an immediate comparison between the effects of a design load based on static or dynamic computations.

Using the Rayleigh model, the results are significantly influenced by the damping for short pulse durations, where differences above 20% are obtained between the damped and the undamped solution. This behaviour is a consequence of the criterion adopted to identify buckling conditions. As maximum out of plane displacements are of concern, a reduction of the peak deflections, an consequently an increase of the dynamic load factor, seems a natural consequence of the introduction of

damping. In any case, the high degree of nonlinearity of the problem is responsible for a relatively complex behaviour of the panel. Sometimes, the number of halfwaves characterizing the deformed shape sometimes changes depending whether damping is included or not. This consideration can help explaining why the introduction of damping can determine an increase of the DLF as expected or, as observed in the range between 2.5 and 5 ms, a slight reduction. It can be noted that the DLF is smaller than unity for time pulses between 5 and 15 ms, meaning that the static buckling load can provide an unconservative prediction. In particular, this pulse range is close to the first period of the panel natural vibration, i.e. 5.92 ms, in agreement with the findings of previous research activities [21, 22]. For time periods above 10 ms, no significant differences are observed.

The deformed configurations at buckling are reported in Figure 13 for three different time periods of 1, 2.5 and 10 ms.

6 Conclusions

The paper described a procedure to estimate the damping properties of composite structures and to account for its effect during the design and the analysis. The procedure relies on DMA tests for the characterization of the material dissipative properties, and finite element analyses for the assessment of the structural response. The approach offers the advantage of requiring the use of simple material coupons, so resulting in a cost-effective procedure.

The possibility of quantifying the dissipation due to the different portions of the structure, as well as of visualizing the contours of the dissipated energy, provides a useful mean to obtain insight into the structural behaviour.

For the panel under investigation, it was possible to ascribe most of the contribution to damping to the local deflections of the stiffener, identifying also the fiber bending as the predominant mechanism involved in the dissipative phenomenon.

The effects of damping were investigated also with respect to the panel dynamic response after introducing the Rayleigh approximation. The results allows to conclude that, for the panel under investigation, the possibility of accounting for dynamic effects and the structural damping does not lead, in general, to a reduction of the design conservativeness. Indeed, the dynamic load factor presents a dependence on the load duration, and the dynamic load factor is higher than the static counterpart only if the load is applied with pulse durations below 2.5 ms. A reduction of conservativeness can then be achieved when the design loads fall in this range of durations.

The proposed design methodology seems a useful mean to obtain more insight into the evaluation of effects due to dynamics and damping.

7 Acknowledgements

The research leading to these results has partially received funding from the European Union's Seventh Framework Programme [FP7/2007-2013] under grant agreement "DAEDALOS - Dynamics in Aircraft Engineering Design and Analysis for Light Optimized Structures" No. 266411.

References

[1] R. Chandra, S.P. Singh, and K. Gupta. Damping studies in fiber-reinforced composites–a review. *Composite Structures*, 46(1):41–51, 1999.

[2] C.T. Sun, J.K. Wu, and R.F. Gibson. Prediction of material damping of laminated polymer matrix composites. *Journal of Materials Science*, 22(3):1006–1012, 1987.

[3] E.E. Ungar and E.M. Kerwin. Loss factors of viscoelastic systems in terms of energy concepts. *The Journal of the Acoustical Society of America*, 34:954–957, 1962.

[4] N. Alam and N.T. Asnani. Vibration and damping analysis of fibre reinforced composite material plates. *Journal of Composite Materials*, 20(1):2–18, 1986.

[5] Y. Othta, Y. Narita, and K. Nagasaki. On the damping analysis of FRP laminated composite plates. *Composite Structures*, 57(1):169–175, 2002.

[6] M. Meunier and R.A. Shenoi. Dynamic analysis of composite sandwich plates with damping modelled using high-order shear deformation theory. *Composite Structures*, 54(2):243–254, 2001.

[7] R.D. Adams and D.G.C. Bacon. Effect of fibre orientation and laminate geometry on the dynamic properties of CFRP. *Journal of Composite Materials*, 7:402–428, 1973.

[8] R.G. Ni and R.D. Adams. The damping and dynamic moduli of symmetric laminated composite beams-theoretical and experimental results. *Journal of Composite Materials*, 18:104–121, 1984.

[9] S.J. Hwang and R.F. Gibson. The use of strain energy-based finite element techniques in the analysis of various aspects of damping of composite materials and structures. *Journal of Composite Materials*, 26(17):2585–2605, 1992.

[10] R.D. Adams and M.R. Maheri. Dynamic flexural properties of anisotropic fibrous composite beams. *Composites Science and Technology*, 50(4):497–514, 1994.

[11] J.H. Yim and B.Z. Jang. An analytical method for prediction of the damping in symmetric balanced laminated composites. *Polymer Composites*, 20(2):192–199, 1999.

[12] R.D. Adams and M.R. Maheri. Damping in advanced polymer–matrix composites. *Journal of Alloys and Compounds*, 355(1):126–130, 2003.

[13] M.R. Maheri. The effect of layup and boundary conditions on the modal damping of frp composite panels. *Journal of Composite Materials*, 45(13):1411–1422, 2011.

[14] J. Li and Y. Narita. Analysis and optimal design for the damping property of laminated viscoelastic plates under general edge conditions. *Composites Part B: Engineering*, 45(1):972–980, 2013.

[15] J.M. Berthelot and Y. Sefrani. Damping analysis of unidirectional glass and kevlar fibre composites. *Composites Science and Technology*, 64(9):1261–1278, 2004.

[16] E.K. Billups and M.N. Cavalli. 2D damping predictions of fiber composite plates: layup effects. *Composites Science and Technology*, 68(3):727–733, 2008.

[17] D.A. Saravanos and C.C. Chamis. Unified micromechanics of damping for unidirectional fiber reinforced composites. TM 102107, NASA, 1989.

[18] D.A. Saravanos and C.C. Chamis. Mechanics of damping for fiber composite laminates including hygro-thermal effects. TM 102329, NASA, 1989.

[19] A.S. Volmir. *The Nonlinear Dynamics of Plates and Shells*. Nauka, Moscow, 1974.

[20] G.J. Simitses. *Dynamic Stability of Suddenly Loaded Structures*. Springer-Verlag, New York, 1990.

[21] T. Weller, H. Abramovich, and R. Yaffe. Dynamic buckling of beams and plates subjected to axial impact. *Computers & Structures*, 32(3):835–851, 1989.

[22] H. Abramovich and A. Grunwald. Stability of axially impacted composite plates. *Composite Structures*, 31(1):151–158, 1995.

[23] C. Bisagni and E. Catapano. Strain energy method to model composite structures damping. In 54^{th} *AIAA/ASME/ASCE/AHS/ASC Structures, Structural Dynamics, and Materials Conference*, AIAA-2013-1760, Boston, MA, 8–11 April 2013.

[24] H. Altenbach, J. Altenbach, and W. Kissing. *Mechanics of Composite Structural Elements*. Springer, Berlin Heidelberg, 2004.

[25] J.D.D. Melo and D.W. Radford. Viscoelastic characterization of transversely isotropic composite laminae. *Journal of Composite Materials*, 37(2):129–145, 2003.

[26] J.N. Reddy. *Mechanics of Laminated Composite Plates and Shells: Theory and Analysis*. CRC Press, Boca Raton, 2004.

[27] J.M. Berthelot. *Dynamics of Composite Materials and Structures*. ISMANS, Institute for Advanced Materials and Mechanics, Le Mans, France, 2007.

[28] K.J. Bathe. *Finite Element Procedures*. Prentice Hall, Upper Saddle River New Jersey, 1996.

[29] E. Riks, C.C. Rankin, and F.A. Brogan. On the solution of mode jumping phenomena in thin-walled shell structures. *Computer Methods in Applied Mechanics and Engineering*, 136(1):59–92, 1996.

[30] M. Hilburger and J.H. Starnes. Buckling behavior of compression-loaded composite cylindrical shells with reinforced cutouts. *International Journal of Non-Linear Mechanics*, 40(7):1005–1021, 2005.

[31] C. Bisagni and P. Linde. Numerical simulation of the structural behaviour of ortothropically stiffened aircraft panels under short time duration loading. In *Proceedings of International Congress of Aeronautical Sciences*, Hamburg, Germany, 3–8 September 2006.

Table 1: Specimen equivalent bending stiffness for different orientation angles θ.

θ	0°	30°	45°	90°
K [N/mm]	285	37	23	16

Table 2: Ply elastic properties.

E_{11} [MPa]	E_{22} [MPa]	G_{12} [MPa]	ν_{12}
155600	8200	4500	0.34

Table 3: Ply specific damping capacities at 50 Hz.

Ψ_{11} [%]	Ψ_{22} [%]	Ψ_{12} [%]
1.42	1.9	8.1

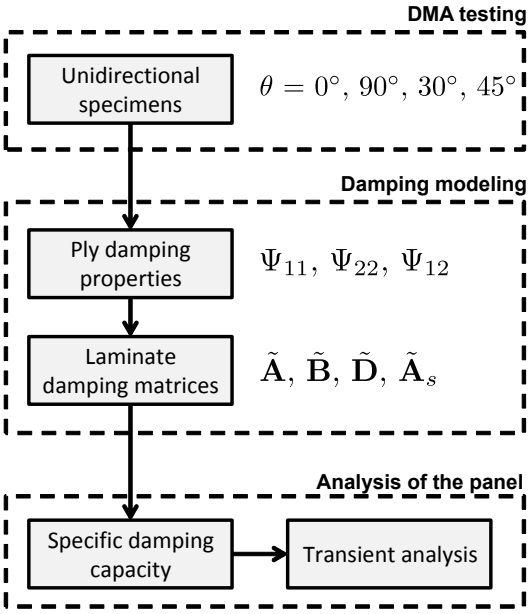

Figure 1: Overview of the procedure.

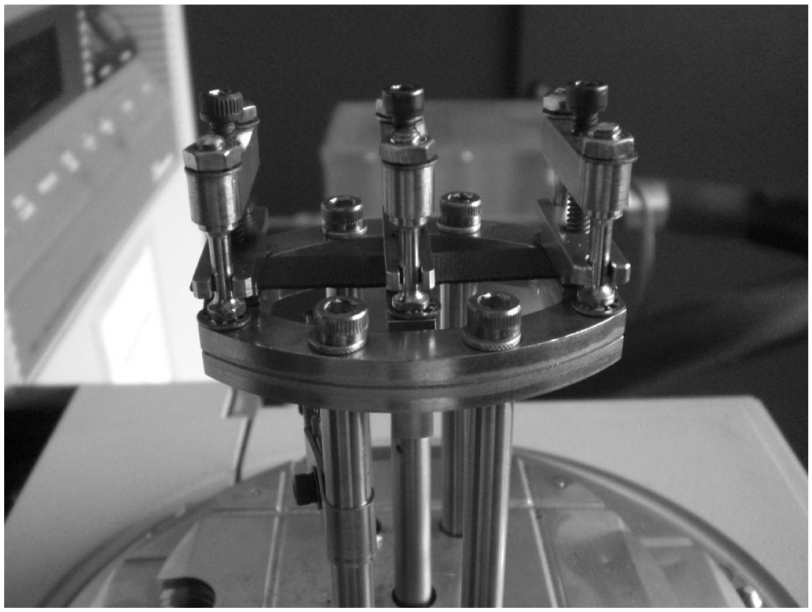

Figure 2: DMA testing equipment in dual cantilever configuration.

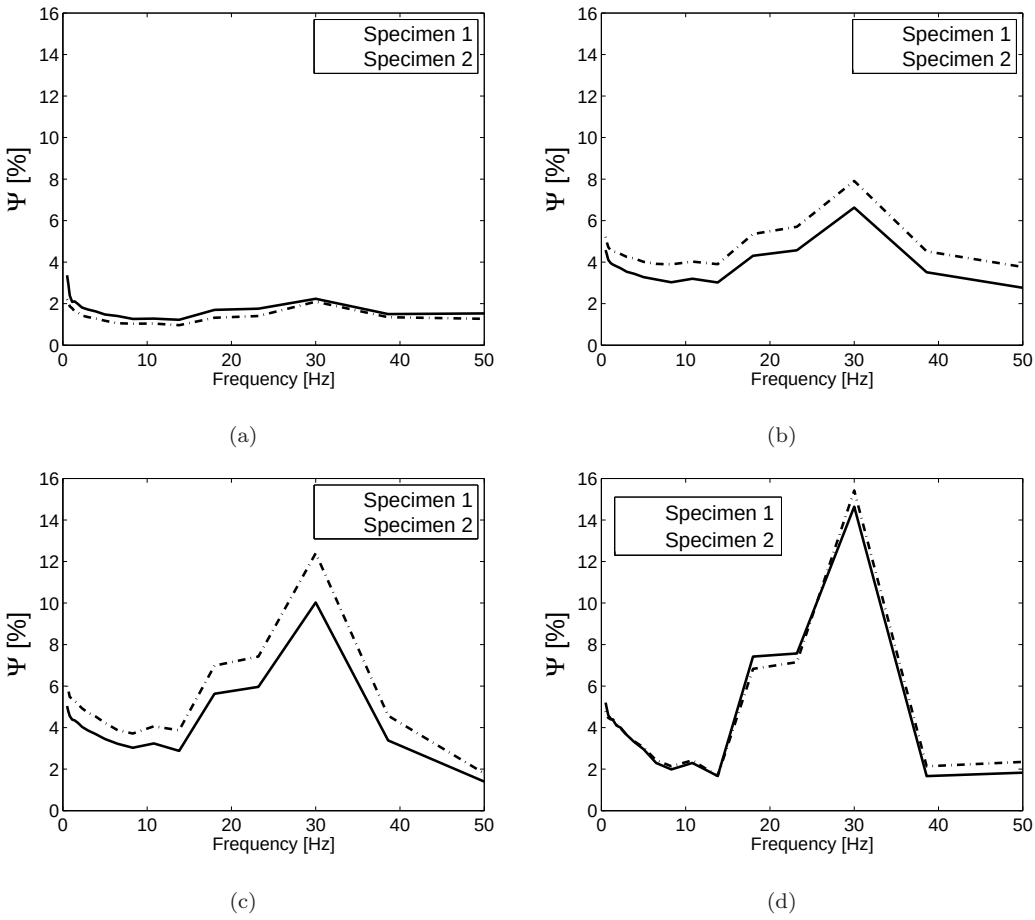

Figure 3: DMA results of two specimens for each configuration: (a) $[0°]_6$, (b) $[30°]_6$, (c) $[45°]_6$, (d) $[90°]_6$.

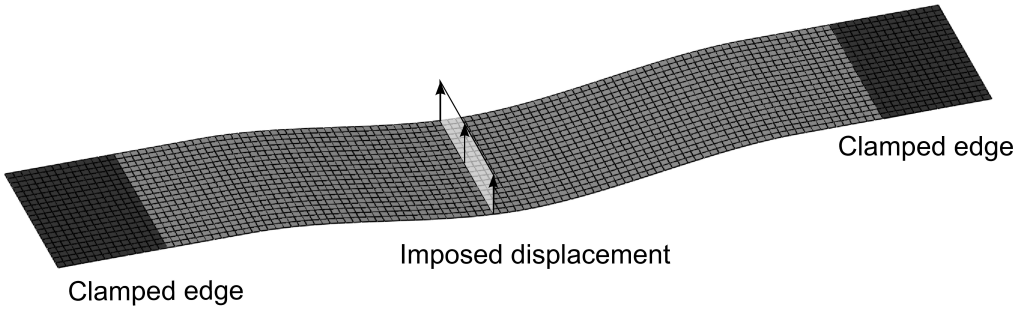

Figure 4: Finite element model of DMA test.

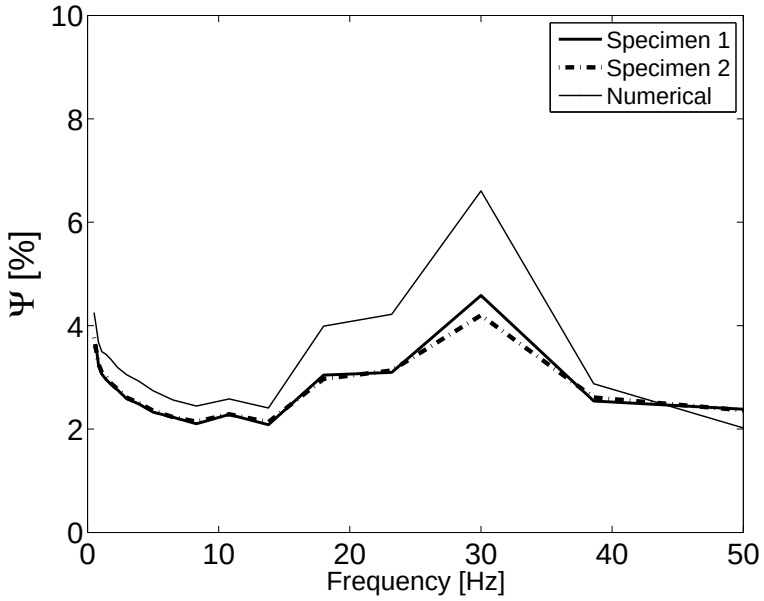

Figure 5: Specific damping capacity of quasi-isotropic specimen.

MODIFIED

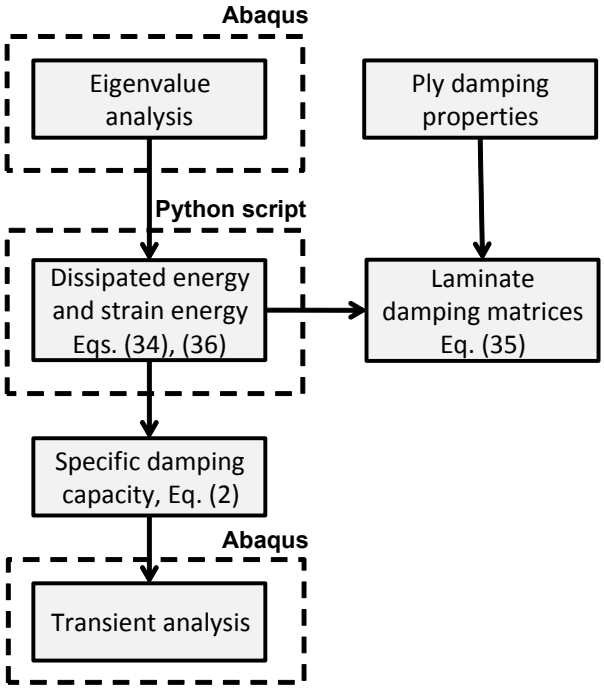

Figure 6: Procedure for panel analysis.

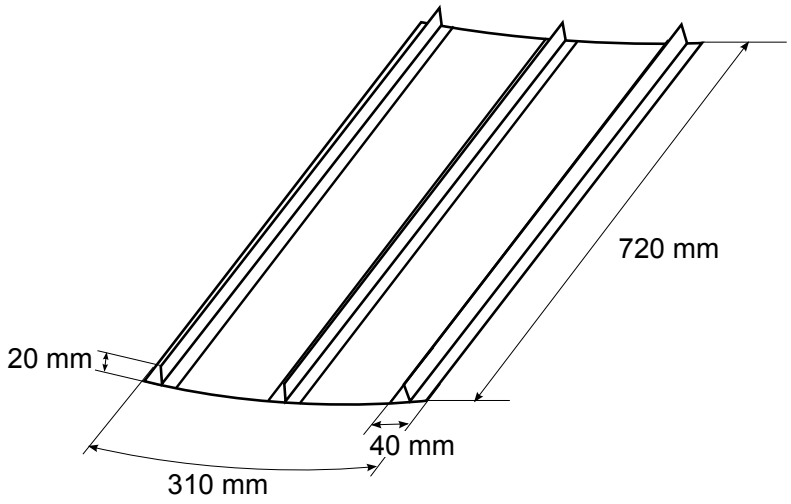

Figure 7: Three-stringer composite panel.

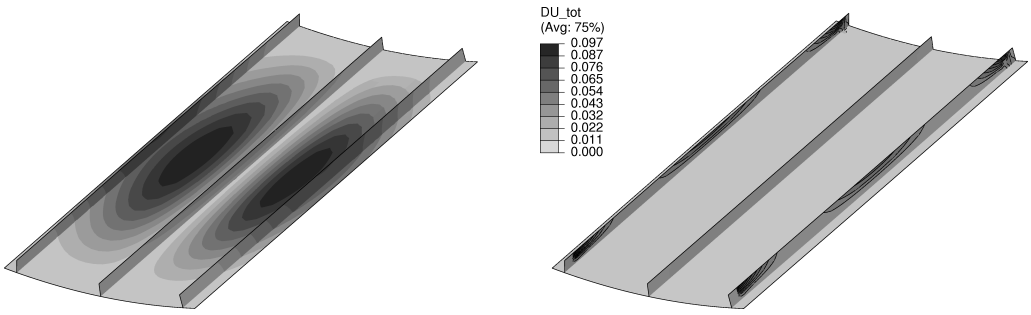

(a) (b)

Figure 8: The three stringer panel: (a) first eigenmode, (b) dissipated energy density.

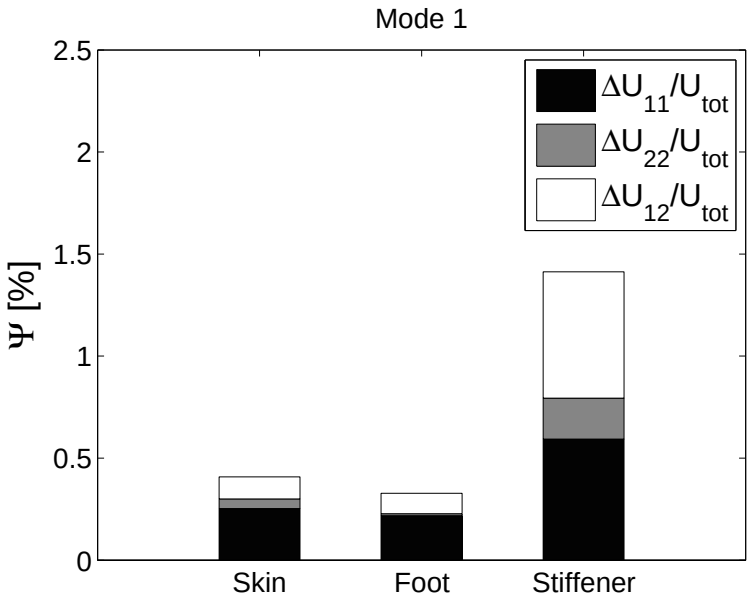

Figure 9: Sub-division of the SDC between the different portions of the structure.

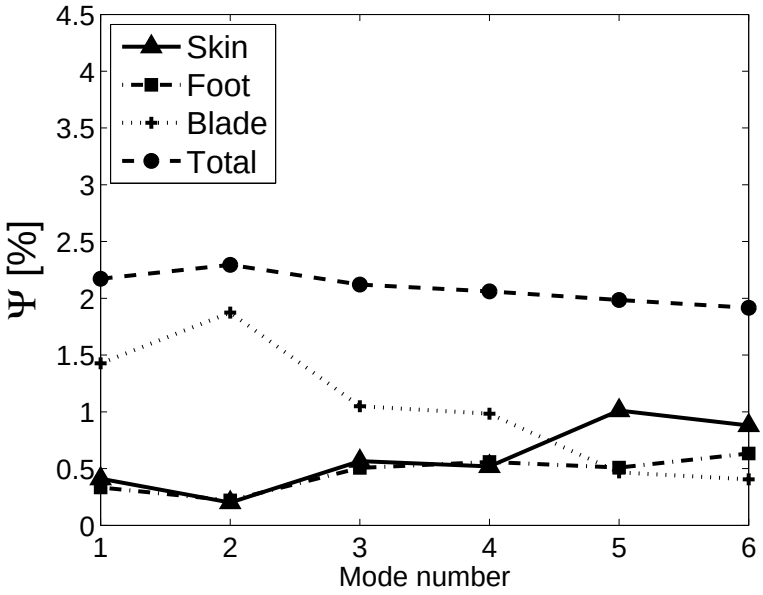

Figure 10: Contribution of different portions of structure to SDC - First six eigenmodes.

MODIFIED

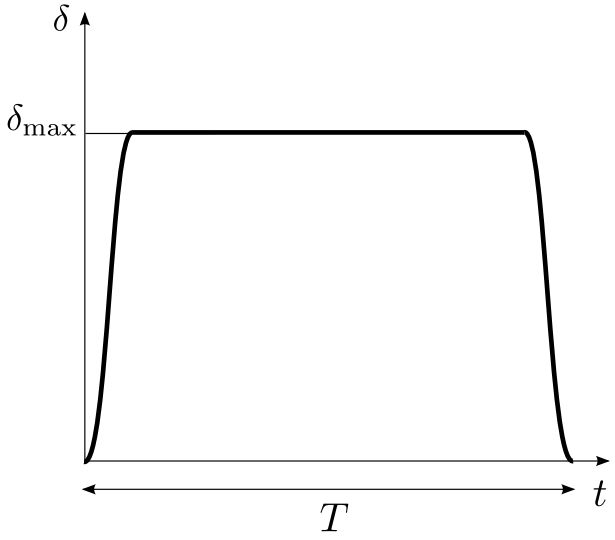

Figure 11: Imposed time-displacement history.

MODIFIED

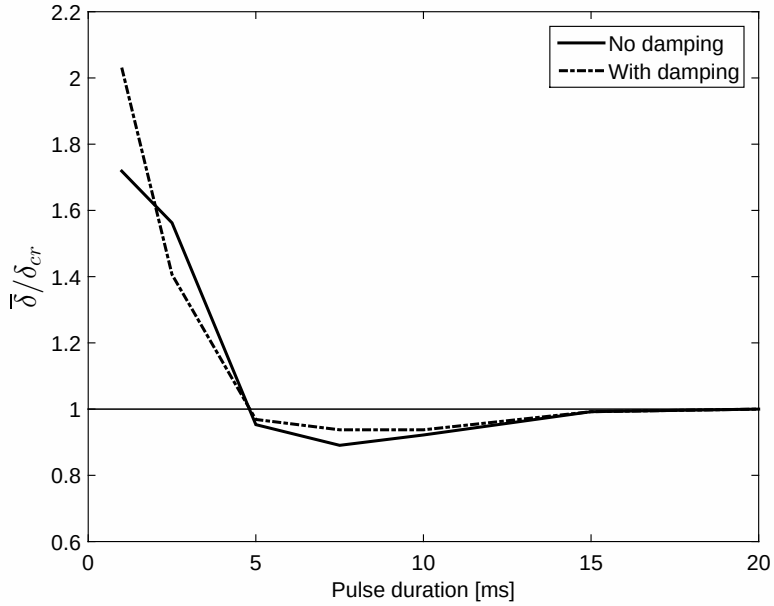

Figure 12: Dynamic load factors.

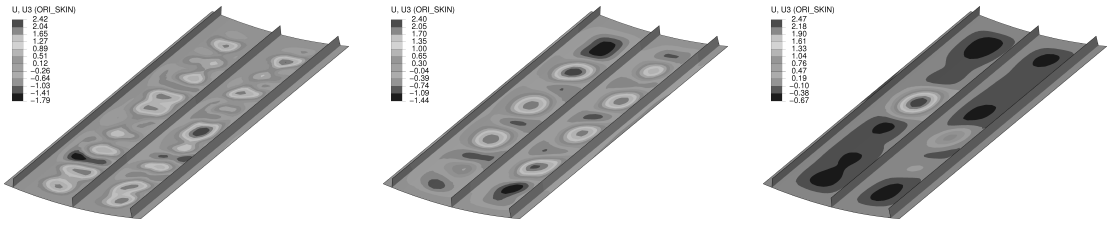

(a) (b) (c)

Figure 13: Deformed shapes for different pulse duration for the panel with damping: (a) 1 ms, (b) 2.5 ms, (c) 10 ms.